Electrocatalysts

International Edition: DOI: 10.1002/anie.201607393
German Edition: DOI: 10.1002/ange.201607393

Facile Synthesis of Black Phosphorus: an Efficient Electrocatalyst for the Oxygen Evolving Reaction

Qianqian Jiang, Lei Xu, Ning Chen, Han Zhang, Liming Dai,* and Shuangyin Wang**

Abstract: *Black phosphorus (BP) as a new 2D material has attracted extensive attention because of its unique electronic, optical, and structural properties. However, the difficulties associated with BP synthesis severely hinder the further development of BP for any potential applications. On the other hand, searching for other potential applications of BP is also a big challenge. A facile strategy was developed for preparation of BP supported on Ti foil (BP-Ti) in a thin-film form. Surprisingly, the as-prepared BP shows advanced electrocatalytic activity for the oxygen evolution reaction (OER). To improve the OER activity of the electrocatalyst, BP was grown on a carbon nanotube network (BP-CNT), showing even better activity. The results demonstrate that BP can be prepared by a facile method and may be applied as an electrocatalyst.*

Elemental phosphorus (P), exists in three allotropes: white (WP), red (RP), and black (BP). Compared to WP, with a high toxicity and low ignition point (ca. 30 °C in moist air),[1] RP and BP are safer to handle. Nevertheless, RP suffers from an extremely low electronic conductivity (1×10^{-14} S cm^{-1}) while BP is the most difficult to synthesize among the three P allotropes, even though BP is thermodynamically more stable than RP under standard conditions.[2] Similar to graphite, BP has recently been recognized as a new member of the 2D material family.[2b] Unlike graphene sheets, with a zero band gap and semiconducting dichalcogenides with an indirect band gap, 2D BP layers have a thickness-dependent direct band gap ranging from 0 to 2 eV.[2b] Furthermore, BP exhibits pressure-induced and temperature-dependent phase transitions among the rhombohedral, semimetallic, and cubic metallic phases,[3] and crystallizes orthorhombically to form puckered layers oriented parallel with respect to the ac plane. Currently, the main strategies to prepare BP include high-energy mechanical milling (HEMM), mineralizer-assisted gas-phase transformation (MGPT), or high-pressure high-temperature (HPHT) conversion from RP.[4] All of these methods are critically dependent on preparative conditions.

BP has attracted a surge of interest as a new 2D building block in field-effect transistors, lithium- and sodium-ion batteries, photocatalysis, and gas sensors.[5] However, as far as we are aware no study on electrocatalysis by BP has been reported, though many semiconducting metal oxides, nitrides, and sulfides have previously demonstrated good activities in the OER.[6] Herein, development of a thermal-vaporization transformation (TVT) method for preparation of BP is described for the first time. The BP materials demonstrated highly efficient OER activities with an onset potential of about 1.48 V (vs. RHE) and a required potential of 1.6 V to achieve a current density of 10 mA cm^{-2}, comparable to commercial RuO_2 electrocatalysts.

BP was prepared by the proposed TVT strategy (Supporting Information, Experimental Section). The RP was pretreated at 200 °C for 2 h to remove surface oxides and contaminants. The thermal annealing of the pretreated RP powder led to its vaporization, initially starting from 450 °C (the vaporization temperature of RP). Subsequent thermal treatment at 650 °C induced a transformation into BP. Compared with traditional BP preparation methods,[4] the TVT method offers a facile approach to BP films or particles supported by electrochemically inert, but electrically conductive substrates, to facilitate electrocatalytic evaluation. Most of the conventional synthetic approaches to BP[4] produce large-sized bulk materials, from which fine particles have to be fabricated by ball-milling or grinding to attain the sort of highly dispersed or even thin-film-type catalysts needed for electrochemical applications. In this regard, our newly developed TVT approach directly produces either supported BP thin films or highly dispersed CNT-supported BP particles, which can be directly used as working electrodes.

Figure 1 shows the scanning electron microscope (SEM) images for the as-synthesized BP-Ti and the bare Ti foil reference. As can be seen, the bare Ti foil has a clean and smooth surface (Figure 1 a) while the BP-Ti shows a surface morphology with well-defined polyhedral structures (Figure 1 b). Under high magnification (Figure 1 c), a uniformly distributed BP texture is clearly evident. The cross-section SEM image given in Figure 1 d shows a thickness of approximately 1.25 μm for the BP thin film on Ti foil. The weight percentage of BP on the Ti foil was determined to be 13.41 wt % by thermal gravimetric analyses (TGA;

[*] Dr. Q. Jiang, L. Xu, N. Chen, Prof. S. Wang
State Key Laboratory of Chem/Bio-Sensing and Chemometrics
College of Chemistry and Chemical Engineering, Hunan University
Changsha, 410082 (P.R. China)
E-mail: shuangyinwang@hnu.edu.cn
Dr. Q. Jiang, Prof. H. Zhang
SZU-NUS Collaborative Innovation Center for Optoelectronic Science and Technology, Key Laboratory of Optoelectronic Devices and Systems of Ministry of Education and Guangdong Province
College of Optoelectronic Engineering, Shenzhen University
Shenzhen 518060 (P.R. China)
E-mail: hzhang@szu.edu.cn
Prof. L. Dai
Department of Macromolecular Science and Engineering
Case Western Reserve University
Cleveland (USA)
E-mail: liming.dai@case.edu

Supporting information for this article can be found under: http://dx.doi.org/10.1002/anie.201607393.

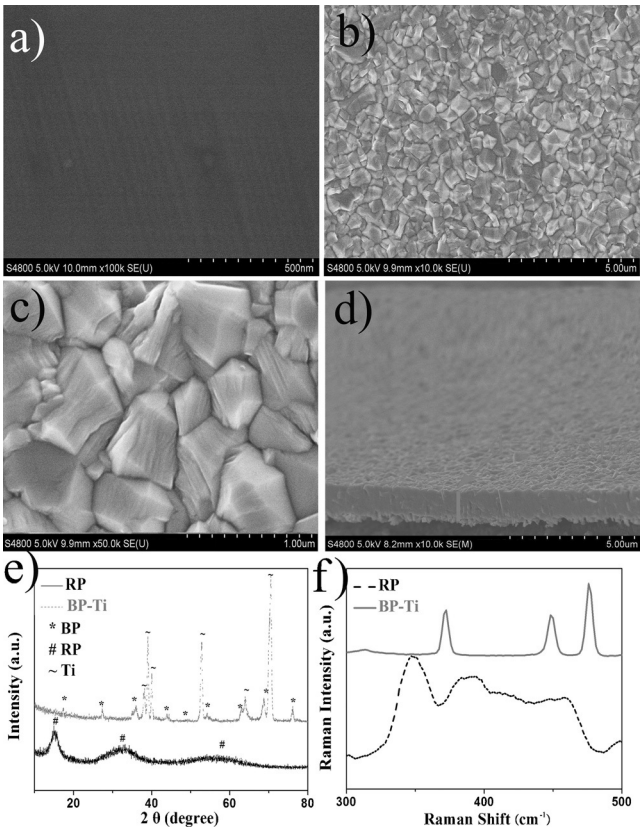

Figure 1. a) SEM image of Ti foil; b, c) SEM images of BP-Ti; d) cross-section of BP-Ti; e) XRD patterns and f) Raman spectra of BP-Ti and RP.

Supporting Information, Figure S1a) to give a mass density of BP on Ti of 12.8 mg cm^{-2}. To further confirm the presence of BP grown on the Ti foil, transmission electron microscopy (TEM), selected-area electron diffraction (SAED) and energy dispersive spectrometer (EDS) mapping of the BP removed from Ti foil are shown in Figure S2 (Supporting Information). As shown in Figures S3–5 (Supporting Information), effects of the annealing temperature, mass loading of RP, and reaction time on the morphology of the resultant BP thin films, were also investigated, indicating wide condition windows for the synthesis of BP films by TVT. The formation of the BP thin film by TVT can be monitored simply by observing the color change from silvery white bare Ti foil (Supporting Information, Figure S6a) to the black color of BP, as confirmed by the scattered debris of BP appearing in the SEM image for a BP-Ti film cut with a sharp knife (Supporting Information, Figure S6b).

A typical XRD pattern of the resultant BP-Ti is given in Figure 1e, along with that of the pretreated RP for comparison. As expected, the XRD pattern of the pretreated RP shows several broad bands of amorphous RP, in good agreement with those previously reported.[7] All the diffraction peaks of the BP-Ti, except those from Ti (JCPDS No. 97-007-6165), can be indexed to an orthorhombic BP with a high degree of crystallization (JCPDS No. 97-009-8119),[8] clearly indicating the formation of the BP on Ti foil. We also investigated the effect of the reaction temperature. As shown in Figure S7 (Supporting Information), all samples show characteristic diffraction peaks, indicating the efficiency of the TVT strategy. The Rietveld refinements of the XRD patterns are shown in Table S1 (Supporting Information). The refined lattice parameters are identical to the reported results.[9] Comparing the lattice parameters, we find that the parameters a, b, and c become larger with temperature.

The successful formation of BP from RP by the TVT approach is further supported by the Raman spectra shown in Figure 1f. While RP shows three characteristic bands between 300 and 500 cm^{-1},[10] the orthorhombic BP reveals three Raman peaks at about 361, 438, and 465 cm^{-1} attributable to A_{1g}, B_{2g}, and A_{2g}, respectively.[7b] Raman spectra for BP-Ti films formed with different mass loadings of RP, different temperatures, and different reaction times (Supporting Information, Figure S8) indicate, once again, wide synthetic windows for the formation of BP by the newly developed TVT approach. The typical XPS spectra of the RP and BP-Ti are shown in Figure S9 (Supporting Information). Three peaks centered at 129.9, 130.3 (shoulder peak), and 134.4 eV are observed in the P 2P XPS spectrum of the RP (Supporting Information, Figure S9a), in agreement with previous reports.[11] Clearly, only two separated peaks centered at 129.3 and 130.5 eV are observed in the P 2P XPS spectrum of the BP-Ti (Supporting Information, Figure S9b), corresponding to the P $2p_{3/2}$ and P $2p_{1/2}$ energies of BP.[12]

Figure 2a shows the electrocatalytic performance for the OER of BP-Ti, RP, and bare Ti in 0.1 M KOH solution. The onset potential for OER on BP-Ti is 1.48 V, which is comparable to most metal oxide-based electrocatalysts.[13] The observed OER current density from the BP-Ti electrode can be exclusively attributed to the BP, as both the Ti foil and residual RP were demonstrated to be inactive for OER (Figure 2a). Systematic linear sweep voltammetry (LSV) measurements on the Ti-supported BP films deposited under different conditions, including different mass loadings of RP, different temperatures, and different reaction times (Supporting Information, Figure S10), indicate that the BP-Ti prepared with 0.5 g of RP at 650 °C for 5 h exhibited the best OER activity. The catalytic kinetics for OER on BP-Ti was examined with Tafel plots.[14] Figure 2b shows a Tafel slope of 91.52 mV dec^{-1}, which is lower than other reported values.[6,15] Therefore, the newly developed BP-Ti holds great promise as an electrocatalyst in the OER. The electrochemical surface area (ECSA) of the BP-Ti is determined to be 6.62 mF cm^2 (Supporting Information, Figure S11). As shown by electrochemical impedance spectroscopy plots in Figure 2c, the ohmic resistance (R_s) for RP is about 58.17 Ω, much larger than that for BP and BP-Ti. The charge transfer resistance (R_{ct}) of the BP-Ti is much smaller than that for RP and bare Ti. The high electrochemical surface area and good electrochemical properties of BP-Ti indicate that this material is highly efficient for the OER. Figure 2d shows the chronoamperometric response for BP-Ti at 1.65 V, demonstrating high stability. After electrochemical testing, the structure is retained well, as evidenced by the XRD patterns collected after testing (Supporting Information, Figure S12a).

Beyond high intrinsic activity, a high surface area and a good electronic conductivity are also essential to high

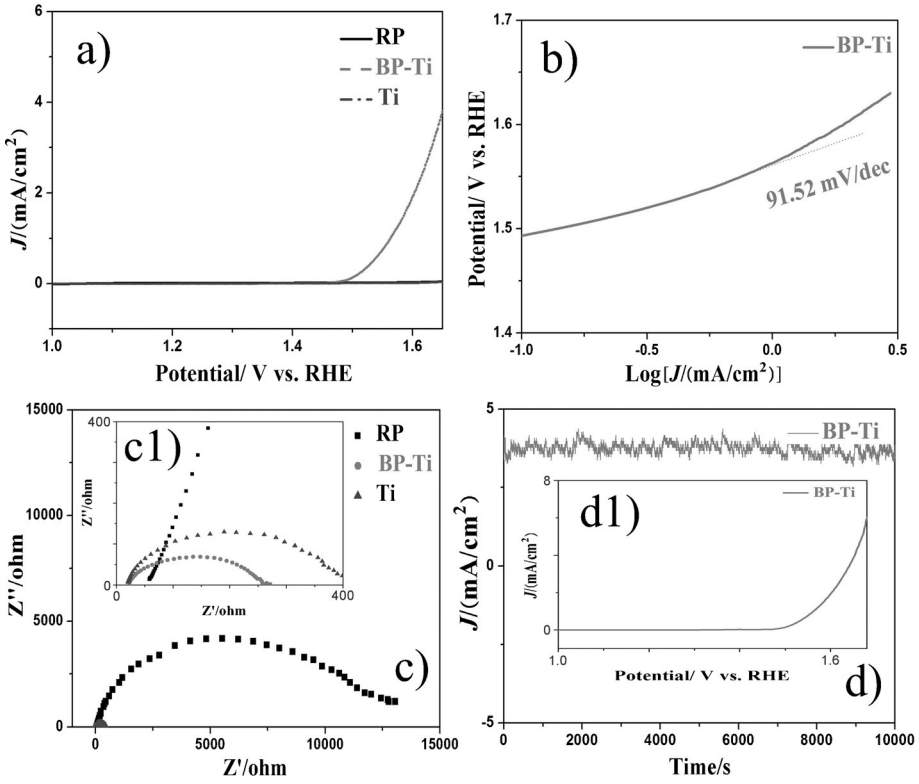

Figure 2. a) Polarization curves of RP, Ti, and BP-Ti in an O_2-saturated KOH solution; b) Tafel plots of BP-Ti; c) electrochemical impedance spectroscopy (EIS) of RP, BP-Ti, and Ti; c1) the magnified EIS; d) chronoamperometric response at 1.65 V; d1) polarization curves of BP-Ti before chronoamperometric response.

activity of an electrocatalyst. Apparently, the above thin-film electrocatalyst (BP-Ti) possesses limited exposed surface sites and relatively poor conductivity for OER because of the bulk nature of the thin-film structure. To further enhance the OER performance of BP electrocatalysts generated by our TVT approach, we used CNT networks with a large surface area and high conductivity as a three-dimensional (3D) support for depositing BP particles by TVT. The pretreated RP was mixed with CNT. With the vaporization of RP above 450 °C, the vaporized P species can diffuse into the CNT matrix uniformly because of the excellent adsorption properties of carbon materials. A high temperature (650 °C) further induces transformation from RP into BP in the CNT matrix. As expected, the SEM image in Figure 3a shows a uniform dispersion of the BP particles within the CNT network with a porous structure. The SEM images of RP, CNT-650, and BP-CNT obtained after reaction over different time periods (Supporting Information, Figure S13) indicate that a reaction time of 5 h produces the best dispersion of BP in a CNT matrix. A time longer than 5 h led to a decrease of the deposited amount of BP. Figure 3b shows a high resolution TEM image for BP-CNT, which clearly reveals the coexistence of a lattice fringe space of 3.36 Å, corresponding to the (002) plane of CNTs[16] and another lattice fringe space of 2.5 Å arising from the (111) plane of BP.[9] The selected area electron diffraction patterns (SAED) reproduced in Figure 3c are assignable to the (021), (041), and (002) planes of the BP crystal, consistent with the well-known BP lattice

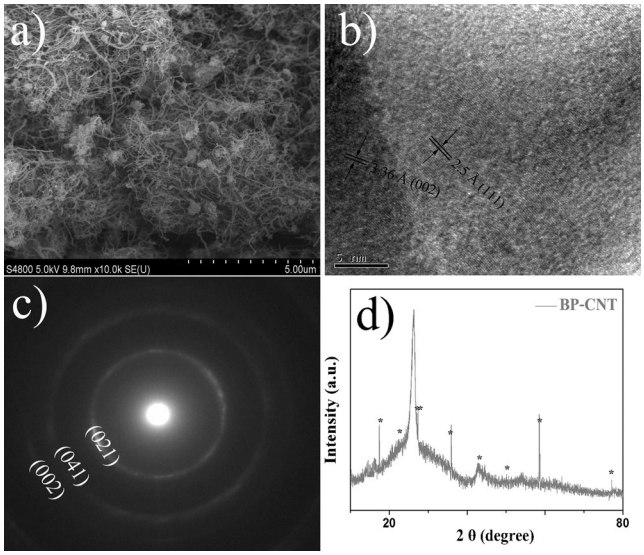

Figure 3. a) SEM and b) HR-TEM images of BP-CNT; c) SAED pattern taken from (b); d) XRD pattern of BP-CNT.

parameters.[9] Furthermore, the TEM image and corresponding EDS elemental mapping of individual BP-CNT bundles given in Figure S14 (Supporting Information) show an intimate contact between BP and the CNT support, an additional advantage for electrochemical applications. The XRD pattern of the BP-CNT given in Figure 3d shows the features associated with the carbon nanotubes (JCPDS 97-007-6767) and orthorhombic BP (JCPDS 97-009-8119)[8] without any other impurity, confirming again the successful preparation of BP nanoparticles on the 3D CNT network support. The XPS spectrum of BP-CNT is given in Figure S9c (Supporting Information). Two separated peaks centered at 129.3 and 130.5 eV are observed in the P 2P spectrum of BP-CNT, corresponding to the P $2p_{3/2}$ and P $2p_{1/2}$ energies of BP.[17] Meanwhile, the P-C peak (at 131.8 eV) was not observed,[6] illustrating that no P atoms were doped into the CNTs. The other peak centered at 134.3 eV is probably due to the adsorption of oxidative radicals.[18]

Figure 4 shows the electrocatalytic OER activities for RP, BP-CNT, and CNT measured in an O_2-saturated 0.1 M KOH. As can be seen in Figure 4a, the onset potential for OER on BP-CNT is 1.49 V versus RHE, which is similar to that for

BP-Ti, indicating the major contribution of BP to the OER. We further compared the potentials required to deliver a 10.0 mA cm^{-2} current density ($E_{j=10}$).[17] BP-CNT only requires 1.6 V (Figure 4a), close to that of commercial IrO_2 (1.57 V) and commercial RuO_2 (1.59 V), and even to potentials required by most metal oxide-based OER electrocatalysts (Supporting Information, Figure S15 and Table S2), suggesting the superior electrocatalytic performance of BP-CNT for the OER. The observed excellent OER performance of BP-CNT can also be exclusively attributed to BP, as both the CNT support and residual RP were demonstrated to be inactive for OER (Figure 4a). As shown in Figure 4b, a lower Tafel slope (72.88 mV dec^{-1}) on BP-CNT is observed with respect to BP-Ti (91.52 mV dec^{-1}), indicating more efficient catalytic kinetics for the former as a consequence of the 3D network structure associated with the CNT support. To further confirm the effect of the CNTs, we performed electrochemical impedance spectroscopic measurements on BP-CNT, RP, and CNT. As can be seen in Figure 4c, the charge transfer resistance (R_{ct}) of BP-CNT ($R_{ct} \approx 191.4\ \Omega$) is much lower than that of BP-Ti ($R_{ct} \approx 263.4\ \Omega$). Similar to BP-Ti, BP-CNT also shows good stability for the OER, as evidenced by the chronoamperometric response at a constant potential of 1.77 V (Figure 4d). In fact, the current density of BP-CNT only decreased by 3.4% after continuous operation for 10000 s, which indicates stability greater than that for BP-Ti (9.48%; Figure 2d). To further illustrate the stability of BP-CNT, an XRD pattern of BP-CNT after the chronoamperometric response is shown in Figure S12b (Supporting Information). As shown, the structure of BP is retained well, indicating excellent structural stability, which was also demonstrated by titration experiments and Fourier transform infrared spectroscopy (Supporting Information, Figure S16). Systematic LSV measurements on BP-CNTs prepared with different mass loadings of RP, at different temperatures, and over different reaction times (Supporting Information, Figure S17), suggest that BP-CNT prepared with a mass ratio of BP/CNT = 10:1, at 650 °C for 5 h, gives the best OER performance. The high double layer capacitance (Supporting Information, Figure S18; 25.42 mF cm^2), which is much higher than that of BP-Ti (6.62 mF cm^2), is intrinsically associated with the 3D CNT network. Finally, we evaluated the OER activity of BP-Ti and BP-CNT in 1 M KOH (Supporting Information, Figure S19), and observed excellent OER activity of BP in concentrated alkaline solutions.

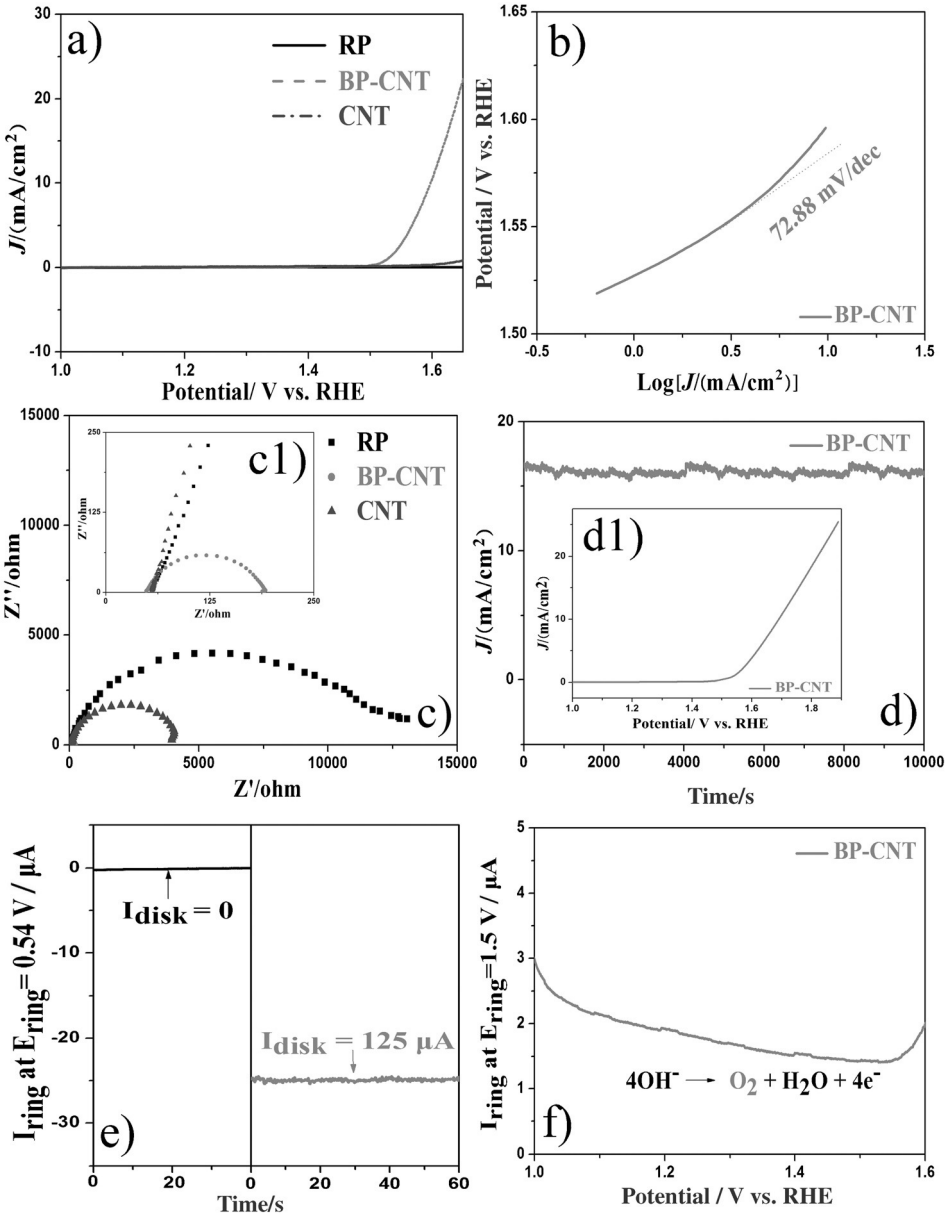

Figure 4. a) Polarization curves of RP, CNT, and BP-CNT in an O_2-saturated KOH solution; b) Tafel plots of BP-CNT; c) EIS of RP, BP-CNT, and CNT; c1) the magnification of EIS (c); d) chronoamperometric response at 1.77 V ($E_{j=16.5}$); d1) polarization curves of BP-CNT before the chronoamperometric response; ring current of BP-CNT on an RRDE (1500 rpm) in e) O_2-saturated and f) N_2-saturated KOH solutions.

To further understand the reaction mechanism, the rotating ring-disk electrode (RRDE) technique was employed with a Pt-ring electrode potential of 1.50 V to analyze the byproduct contents (peroxide intermediates) formed at the surface of the BP-CNT catalyst during the OER process. Figure 4e shows a relatively low ring current (μA

scale) which is three orders of magnitude lower than that of the disk current (mA scale), suggesting that the rapid increase of current density can be mainly attributed to a four-electron transfer pathway. In the case of the OER process a four-electron transfer pathway is desirable for water oxidation into O_2 with negligible hydrogen peroxide formation. Additionally, the ring current gradually decreased from low to high potential, suggesting that fewer peroxide intermediates formed at the high potential region. Furthermore, to ensure that the observed oxidation current is generated from oxygen evolution, we used a rotating Pt-ring electrode held at the ORR potential of 0.54 V (versus RHE) to detect O_2 generated at the catalyst by electrochemical reduction (Figure 4 f). Firstly, an RRDE with a ring electrode was used to carry out a continuous OER (disk electrode)–ORR (ring electrode) process. The disk current was fixed at 125 μA to generate O_2 molecules from the BP-CNT catalyst, and then the O_2 molecules were further reduced by sweeping across the surrounding Pt-ring electrode with an ORR potential of 0.54 V versus RHE. Consequently, a ring current of approximately 24.56 μA was detected (Figure 4 f) with a high Faradaic efficiency of 98.24%. This result confirms that BP-CNT is able to mediate a fast four-electron reaction to generate O_2 at a relatively low potential.

In summary, for the first time orthorhombic BP was directly grown on a Ti foil and CNT matrix by a novel thermal-vaporization transformation approach. This TVT method can produce BP in various forms, including BP thin film and BP particles on supports. For BP thin-film formation, Ti foil was used as the collecting substrate for the deposition of the vaporized BP species. On the other hand, BP particles could be prepared in a CNT interconnected matrix because of the excellent adsorption properties of carbon materials. BP-CNT demonstrates better dispersion and conductivity than BP-Ti. Interestingly, BP in the form of either BP-Ti or BP-CNT exhibited efficient OER activity, which is even comparable to that of commercial RuO_2 electrocatalysts. This is the first work demonstrating a novel electrocatalytic application of BP. Thus, the facile, but efficient and scalable TVT approach holds great promise for the development of low-cost and effective BP electrocatalysts for OER in metal-air batteries and water-splitting devices.

Experimental Section

Preparation and characterization of catalysts: Prior to BP synthesis, RP (2 g) was pretreated at 200 °C for 2 h. Thereafter, the powder was transferred into a mortar for grinding for about 15 min. To synthesize BP-Ti, the pretreated RP was put in a tube furnace near bare Ti foil. Ar gas with a flow rate of 5 $cm^3 min^{-1}$ was then introduced into the tube furnace at 650 °C for 5 h. Subsequently, the temperature of the tube furnace was reduced to 350 °C for 2 h. For the synthesis of BP-CNT, the pretreated RP and the commercial carbon nanotubes with a mass ratio of 10:1 were mixed and ground together for 15 min. The mixture was placed in a tube furnace, followed by introduction of Ar gas with a flow rate of 5 $cm^3 min^{-1}$ at 650 °C for 5 h. Thereafter, the temperature of the tube furnace was decreased to 350 °C for 2 h. For consistent comparison, CNT was also treated at 650 for 5 h (with product denoted as CNT-650).

Acknowledgements

The work was supported by the National Natural Science Foundation of China (grant no.: 51402100, 21573066, and 61435010).

Keywords: black phosphorus · electrocatalysts · metal-free catalysts · oxygen evolution · vaporization techniques

How to cite: *Angew. Chem. Int. Ed.* **2016**, *55*, 13849–13853
Angew. Chem. **2016**, *128*, 14053–14057

[1] J. A. Young, *J. Chem. Educ.* **2004**, *81*, 946–946.
[2] a) N. Eckstein, A. Hohmann, R. Weihrich, T. Nilges, P. Schmidt, *Z. Anorg. Allg. Chem.* **2013**, *639*, 2741–2743; b) H. O. H. Churchill, J. H. Pablo, *Nat. Nanotechnol.* **2014**, *9*, 330–331.
[3] J. C. Jamieson, *Science* **1963**, *139*, 1291–1292.
[4] a) C. M. Park, H. J. Sohn, *Adv. Mater.* **2007**, *19*, 2465–2468; b) L. Q. Sun, M. J. Li, K. Sun, S. H. Yu, R. S. Wang, H. M. Xie, *J. Phys. Chem. C* **2012**, *116*, 14772–14779; c) M. Köpf, N. Eckstein, D. Pfister, C. Grotz, I. Kruger, M. Greiwe, T. Hansen, H. Kohlmann, T. Nilges, *J. Cryst. Growth* **2014**, *405*, 6–10.
[5] a) A. Favron, E. Gaufres, F. Fossard, A. L. Phaneuf-L'Heureux, N. Y. W. Tang, P. L. Levesque, A. Loiseau, R. Leonelli, S. Francoeur, R. Martel, *Nat. Mater.* **2015**, *14*, 826; b) H. T. Yuan, X. G. Liu, F. Afshinmanesh, W. Li, G. Xu, J. Sun, B. Lian, A. G. Curto, G. J. Ye, Y. Hikita, Z. X. Shen, S. C. Zhang, X. H. Chen, M. Brongersma, H. Y. Hwang, Y. Cui, *Nat. Nanotechnol.* **2015**, *10*, 707–713; c) Z. B. Yang, J. H. Hao, S. G. Yuan, S. H. Lin, H. M. Yau, J. Y. Dai, S. P. Lau, *Adv. Mater.* **2015**, *27*, 3748–3754.
[6] J. T. Zhang, Z. H. Zhao, Z. H. Xia, L. M. Dai, *Nat. Nanotechnol.* **2015**, *10*, 444–452.
[7] Q. Jiangfeng, Q. Dan, A. Xinping, C. Yuliang, Y. Hanxi, *Chem. Commun.* **2012**, *48*, 8931–8933.
[8] R. W. Keyes, *Phys. Rev.* **1953**, *92*, 580–584.
[9] R. Ahuja, *Phys. Status Solidi* **2003**, *235*, 282–287.
[10] S. W. Kim, D. H. Seo, X. Ma, G. Ceder, K. Kang, *Adv. Energy Mater.* **2012**, *2*, 710–721.
[11] J. Song, Z. Yu, M. L. Gordin, X. Li, H. Peng, D. Wang, *ACS Nano* **2015**, *9*, 11933–11941
[12] a) N. B. Goodman, L. Ley, D. W. Bullett, *Phys. Rev. B* **1983**, *27*, 7440–7450; b) A. H. Woomer, T. W. Farnsworth, J. Hu, R. A. Wells, C. L. Donley, S. C. Warren, *ACS Nano* **2015**, *9*, 11933–11941.
[13] Z. Y. Lu, H. T. Wang, D. S. Kong, K. Yan, P. C. Hsu, G. Y. Zheng, H. B. Yao, Z. Liang, X. M. Sun, Y. Cui, *Nat. Commun.* **2014**, *5*, 4345.
[14] S. Fang, H. Xile, *J. Am. Chem. Soc.* **2014**, *136*, 16481–16484.
[15] S. Chen, J. J. Duan, M. Jaroniec, S. Z. Qiao, *Adv. Mater.* **2014**, *26*, 2925–2930.
[16] a) P. Trucano, R. Chen, *Nature* **1975**, *258*, 136–137; b) K. Youngjin, P. Yuwon, C. Aram, C. Nam-Soon, K. Jeongsoo, L. Junesoo, R. J. Heon, S. M. Oh, L. Kyu Tae, *Adv. Mater.* **2013**, *25*, 3045–3049.
[17] C. C. L. Mccrory, J. Suho, J. C. Peters, T. F. Jaramillo, *J. Am. Chem. Soc.* **2013**, *135*, 16977–16987.
[18] W. Junli, Y. Qing, Z. Zude, S. Shouheng, *Chem. Eur. J.* **2010**, *16*, 7916–7924.

Received: July 30, 2016
Revised: August 28, 2016
Published online: September 29, 2016

